Eur Biophys J (1999) 28: 112–118 

ARTICLE

**Chun-Min Lo · Jack Ferrier**

# Electrically measuring viscoelastic parameters of adherent cell layers under controlled magnetic forces

Received: 23 March 1998 / Revised version: 23 June 1998 / Accepted: 1 July 1998

**Abstract** Electrical cell-substrate impedance sensing (ECIS) was used to measure the time-dependence and frequency-dependence of impedance for current flowing underneath and between cells. Osteosarcoma cells with a topology similar to a short cylinder (coin-like) surmounted by a dome were used in this study. Application of a small step increase in net vertical stress to the cells (4 and 7 dyn/cm$^2$), via magnetic beads bound to the dorsal (upper) surface, causes an increase in cell body height and an increase in cell-cell separation, as well as stretching of the cell-substrate adhesion bonds. This results in a fast drop in measured resistance (less than 2 s), followed by a slower change with a time constant of 60–150 s. This time constant is about 1.5 times longer at 22 °C than that at 37 °C; it also increases with applied stress. Our frequency scan data, as well as our data for the time course of resistance and capacitance, show that the fast change is associated with both the under-the-cells and between-the-cells resistance. The slower change in resistance mainly reflects the between-the-cells resistance. To obtain viscoelastic parameters from our data we use a simple viscoelastic model comprising viscous and elastic elements (i.e., a dashpot and two springs) for the cell body, and an elastic element (a spring) for the cell-substrate adhesion system. Our results show that the spring constants and the viscosity of the cell body components of this viscoelastic model decrease as the temperature increases, whereas the elastic modulus of cell-substrate adhesion increases with temperature. At 37 °C, for the cell body we obtain a value of about $10^5$ P for the viscous element of the viscoelastic model, and a spring constant expressed in units of an elastic modulus of about $10^4$ dyn/cm$^2$ for the spring in series with the viscous element, with another spring with a modulus of about $2\times10^3$ dyn/cm$^2$ in parallel with these. In comparable units, we have a modulus for the cell-substrate adhesion system of about $3\times10^3$ dyn/cm$^2$.

C.-M. Lo · J. Ferrier (✉)
MRC Group in Periodontal Physiology,
4384 Medical Sciences Building, University of Toronto,
Toronto, Ontario M5S 1A8, Canada
e-mail: j.ferrier@utoronto.ca

**Key words** Cellular viscoelasticity · Time-dependent impedance · Electrical cell-substrate impedance sensing · Applied force · Magnetic beads

## Introduction

Viscoelasticity is a general mechanical property of living cells and plays an important role in cell behavior, including development of shape, proliferation, and movement (Elson 1988; Ingber et al. 1994). A well-known example is the leukocyte, which is able to actively deform for penetration of capillaries or for phagocytosis. Recently, Chen et al. (1997) have shown that the extent of cell spreading directly affects the proliferation and survival of fibroblasts, indicating that regulation of cell morphology is critical for cell health. Investigating the viscoelastic properties of cells will enhance our understanding of these essential cellular functions.

The viscoelastic properties of whole cells have been studied using methods such as micropipette aspiration to produce stress (Evans and Yeung 1989; Sato et al. 1996), or manipulation of microplates to which cells have adhered to produce strain (Thoumine and Ott 1997). In this paper we use an electrical method, electric cell-substrate impedance sensing (ECIS), to measure stress-induced mechanical strain of adherent cells. In our measurements, cell layers are cultured on small gold electrodes and the electrical impedance of the cell-covered electrode can be measured as a function of time or of frequency. Collagen-coated ferric oxide beads attached to integrin receptors in the dorsal (upper) cell surfaces are used to apply stress to osteoblast-like ROS 17/2.8 cells. The magnitude of the net applied force is controlled by the number of permanent magnets (one or two), applying an average 4 or 7 dyn/cm$^2$ of stress to each cell.

Comparing measured frequency-dependent data with values obtained from a theoretical cell-electrode model, both junctional resistance and average cell-substrate separation can be determined at steady state (Giaever and

Keese 1991; Lo et al. 1995, 1998). That is, since cells constrain the current flow, the measured electrical impedance is dependent on the space between the cells and on the space between cells and their substrate. We showed in a previous study that this method can detect changes as small as a few nanometers in cell-substrate and cell-cell separation (Lo et al. 1998). In the present study, by analyzing the measured time-dependent impedance obtained during the force-induced step increase in cellular stress, as well as the steady-state frequency-dependent impedance, we are able to determine the parameters of our viscoelastic model. We use units of elastic modulus (stress/strain = force/area) for the spring constants in the viscoelastic model, and units of viscosity (force × time/area) for the viscous element in that model, so that we can compare to the results of other workers such as Sato et al. (1996) and Thoumine and Ott (1997).

## Materials and methods

### Cell culture

Rat osteosarcoma cells (ROS 17/2.8) were cultured at 37 °C in a 5% $CO_2$ incubator, in α-minimal essential medium ($\alpha$-MEM, Gibco, Toronto) with 10% fetal bovine serum (Gibco) and antibiotics. These cells have many osteoblast-like properties (Majeska and Rodan 1982; Ferrier et al. 1987). They also have a topology resembling a short cylinder surmounted by a dome-like section of a spherical surface. Twenty-four hours after inoculating cells into electrode-containing wells, the normal culture medium was changed to $\alpha$-MEM without bicarbonate and with 25 mM HEPES buffer, for measurements at 22 °C or 37 °C.

### Impedance measurements

Frequency scan and time-dependent impedance measurements, and the ECIS model equations, were described in our previous papers (Lo et al. 1994, 1995, 1998). A detailed description of the current pathways under and between the cells is in Lo and Ferrier (1998). Electrode arrays, relay bank, lock-in amplifier, and software for the ECIS measurement were obtained from Applied BioPhysics (Troy, New York). Each electrode array consists of five wells which are 1 cm in height and 0.5 $cm^2$ in area; each well contains a 250-μm-diameter gold electrode and a much larger gold counter electrode.

The amplitude of the alternating current passing through the electrode is 0.09 μA at 22 Hz, increasing with frequency to 1.2 μA at 90 kHz. This produces an amplitude for the alternating voltage drop across the cell layer of about 0.5 mV at 22 Hz, increasing to 6 mV at 90 kHz (half of this voltage drop will be across the top cell membrane, and half across the bottom cell membrane). This is too small to have any known effect on the cells: even a possible small influence on ion flux through open ion channels would be cancelled by the alternating nature of the voltage drop.

The amplitude of the alternating voltage drop at the electrode surface (across the electrode-electrolyte interface) is 28 mV at 22 Hz, falling off with increasing frequency: 12 mV at 44 Hz, 6 mV at 88 Hz, down to 2 mV at 4000 Hz, and 1 mV at 90 kHz. These voltage drops are far too low to produce any electrochemical effects at the electrodes.

The ECIS analysis provides morphological parameters of cell layers such as junctional resistance between cells ($R_b$) and the average cell-substrate separation ($h$). Making measurements at 13 different frequencies during a frequency scan allows a much better fit of the theoretical ECIS model curves to the measured impedance data than does measurement at a single frequency, but this requires about 2 min for each electrode. On the other hand, time-dependent impedance measurements can provide time-dependent resistance and capacitance of a cell-covered electrode every second, but only at a single frequency. We make time-dependent measurements at 4000 Hz, because at this frequency the difference between the resistance of the cells plus electrode and the cell-free electrode is greatest (i.e., the normalized resistance is greatest). This provides the greatest sensitivity for the ECIS analysis, including the resistance versus capacitive reactance plots to be described below. We express $R_b$ as a specific resistance by multiplying the resistance attributable to the junctional (between-the-cells) current flow pathway by the total cell area, $A$ (i.e., by the area of the small electrode, which is about 0.0005 $cm^2$). The resistance attributable to the between-the-cells pathway for a single cell can thus be obtained by dividing $R_b$ by the horizontal area of a single cell, $A_c$ (about 800 $\mu m^2$). In the theoretical ECIS model we employ here, the horizontal section of the cell is assumed to be circular, which is a good approximation to the ROS cells. Using other assumptions regarding horizontal section would give different values for $R_b$ and $h$ (Lo and Ferrier 1998).

### Magnetic beads and force generation

Ferric oxide beads were coated with collagen and the magnetic field was provided by one or two permanent magnets as we described before (Glogauer and Ferrier 1998; Lo et al. 1998). Briefly, ferric oxide beads ($Fe_3O_4$, Aldrich, Milwaukee, Wis.) were coated with collagen by incubating 0.4 g of beads at 37°C for 1 h in a solution comprising 1 ml collagen solution (3 mg/ml; Vitrogen, Collagen Corp., Palo Alto, Calif.) and 100 μl 1 N NaOH. The beads were then washed and equilibrated with phosphate buffered saline. Following sonication to eliminate clumping, beads were added to measuring wells containing substrate-attached cells for 10 min. The cell layer was then washed thoroughly to remove unbound beads. A ceramic permanent magnet provided the magnetic field (Duramax 8, Dura Magnetics, Sylvania, Ohio: a rectangular parallelepiped, 25×101×152 mm, with the larger surfaces being the pole faces). The topological relation between the permanent magnet, the magnetic beads, the cells, and the substrate was illustrated in Lo et al. (1998).

The collagen-coated beads are bound by integrin receptors in the dorsal (upper) plasma membrane, and there is a clustering of attachment points of the cytoskeletal actin microfilaments to integrin receptors binding the beads (Glogauer et al. 1997; Glogauer and Ferrier 1998). The force applied by the beads will thus be transmitted to the cytoskeleton (Glogauer et al. 1997, 1998), and through the cytoskeleton to the integrin-ligand adhesion bonds that attach the cell to substrate (Lo et al. 1998). Part of this force could conceivably also be transmitted to and through the cortex on the upper, lower, and lateral cell surfaces.

Force per unit volume of bead was directly measured by electronic balance, and also calculated from the measured field of the permanent magnet (Glogauer and Ferrier 1998). As previously described, the distribution of bead diameters was measured and used to obtain number-weighted averages for bead diameter (2.5 μm), cross-sectional area (7.0 $\mu m^2$), and volume (21.0 $\mu m^3$). There will be a variation of force per cell because of the variable size of the beads, and the variable number of beads per cell. Taking into account both factors, for a 50% bead coverage of the upper cell surface, the standard deviation of the distribution of force per cell should be 33% of the mean value (Glogauer and Ferrier 1998).

The mean value will be 320 pN of upward force per cell with a single magnet with a pole face 2 cm from the cell layer, and 560 pN with two magnets. Converted to units of stress (force per unit area), these forces produce a net vertical stress in the cells of approximately 4 and 7 dyn/$cm^2$. These forces are less than 10% of the force required to remove fibroblasts from a fibronectin-covered substrate (Lotz et al. 1989), and they do not detach cells in our experiments. The upward magnetic force exerted by a single bead of average volume is less than 5 pN (Glogauer and Ferrier 1998). If this force is applied to a single actin filament of 4 μm length (say a vertical filament stretched between the upper and lower cell surfaces), the spring constant of the filament would be 0.75 pN $nm^{-1}$ (Lo et al. 1998) and the change in filament length would be less than 7 nm.

## Viscoelastic modeling

To characterize the viscoelastic properties of the cell body we use a model that has been used in other studies of cell body viscoelasticity (Schmid-Schönbein et al. 1981; Sato et al. 1996; Thoumine and Ott 1997). This model consists of a Maxwell body (a spring and dashpot in series, with parameters $k_2$ and $\eta$) in parallel with another spring ($k_1$). To describe the elasticity of the cell adhesion system (integrin-adhesion molecule complexes), we use a spring ($k_0$) in series with the system for the cell body. This viscoelastic model is shown in Fig. 1a. Figure 1b shows a theoretical time-dependent strain curve following application of and removal of a constant stress. In this paper, we use units of elastic modulus (force/area) for the $k$ values of the springs, and units of viscosity for the dashpot, to allow

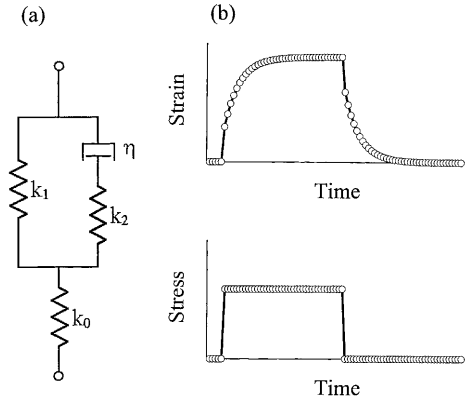


**Fig. 1** **a** Viscoelastic model for an adherent ROS cell, in which the springs represent elasticity and the dashpot represents viscosity. A spring ($k_1$) connected in parallel with a Maxwell body, which consists of a spring ($k_2$) and a dashpot ($\eta$) in series, is used to describe the viscoelasticity of the cell body, and another spring ($k_0$) in series with the cell body system is used to describe the elasticity of cell-substrate adhesion. **b** Time-dependent strain produced by a constant applied stress, calculated from the model shown in **a**. According to this model, the instantaneous elastic response of the cell to an applied vertical force comes from both the cell-substrate adhesion strain, $\Delta h/H$, and the instantaneous vertical strain of the cell body, $\Delta H(t{=}0)/H$, while the retarded strain results solely from the time-dependent vertical strain of the cell body, $\Delta H(t)/H$

comparison to the results of others. We also investigate the question of model dependency of these parameters by obtaining values using another viscoelastic model based on the Kelvin-Voigt body (Haddad 1995).

The elastic strain of the cell adhesion system can be described as

$$\frac{\Delta h}{H} = \frac{\sigma}{k_0} \tag{1a}$$

where $\sigma$ is the applied stress, $h$ is the cell-substrate distance, and $H$ is the vertical height of the cell body. We define $k_0$ in this way to make it comparable to the other $k$ values. The elastic modulus of the adhesion system with strain defined in the more conventional manner as $\Delta h/h$ will thus be $k_0 h/H$. The spring constant of the adhesion system in units of force per unit displacement, per cell, as used by Lo et al. (1998), is then given by $A_c k_0/H$, where $A_c$ is horizontal area per cell.

The time-dependent vertical strain of the cell body can be described as

$$\frac{\Delta H(t)}{H} = \frac{\sigma}{k_1}\left(1 - \frac{k_2}{k_1 + k_2}\,\mathrm{e}^{-t/\tau}\right) \tag{1b}$$

where

$$\tau = \eta\left(\frac{1}{k_1} + \frac{1}{k_2}\right) \tag{2}$$

It should be noted that $\Delta H(t{=}0)/H = \sigma/(k_1{+}k_2)$ and $\Delta H(t \gg \tau)/H = \sigma/k_1$.

Before assessing all four parameters in our viscoelastic model, we need to make some assumptions regarding how a change of junctional resistance between cells, $R_b$, relates

to vertical strain of the cell body. From the definition of $R_b$,

$$\frac{\rho l}{2\pi r_c \frac{w}{2}} = \frac{R_b}{\pi r_c^2} \tag{3}$$

where $l$ and $w$ are the length and the width of the space between cells, and $r_c$ is the radius of the ventral (lower) surface of the cell. The value of $r_c$ is about 16 μm for ROS cells, while $w$ is approximately 30 nm. At 37°C, the medium resistivity, $\rho$, is 54 Ω cm and $R_b$ is about 1.4 Ω cm$^2$, so the value of $l$ can be estimated as 0.5 μm. We assume that the length of junctional resistance channels, $l$, is independent of the applied force, since our force levels are quite small. We also have:

$$\Delta r_c = -\Delta\left(\frac{w}{2}\right) \tag{4}$$

To relate changes in cell morphology to our measured changes in $R_b$ we must make a further assumption about cell shape. If we make the fairly realistic assumption concerning the ROS cells used in this study, that they have a short cylindrical (coin-like) base surmounted by a dome whose surface is part of a sphere, we have:

$$V = \frac{\pi}{6}(H-l)(3r_c^2 + (H-l)^2) + \pi r_c^2 l \tag{5}$$

where $V$ is the cell volume, $H$ is the total height of the cell body, and $l$ is the height of the base (Korn and Korn 1967).

Combining Eqs. (3), (4), and (5) yields a relation between the changes in $H$ and $R_b$:

$$\frac{\Delta H}{H} = \beta\rho l\Delta\left(\frac{1}{R_b}\right) \tag{6}$$

where $\beta$ is between 0.5 and 2. It is straightforward to show that $\beta$ will be between 1 and 2 for cells with $H \ll r_c$, which describes the morphology of our cells. If we also have $l \ll H$, which is a good approximation for our cells, $\beta$ would be close to 1, while for $l \approx H$, $\beta$ would be close to 2. Equation (6) is based on the assumption of constant cell volume. This is a valid assumption for the small applied stresses we use here: these stresses should produce a water flow across the cell membrane that results in a relative cell volume change that is less than 1% of our calculated $\Delta H/H$ values. Furthermore, for the geometrical parameters of our cells, if $l$ was allowed to be an additional variable in Eqs. (3) and (5), there would be no significant change in Eq. (6). This equation provides the link between the viscoelastic model and our impedance measurements.

## Results and discussion

Figure 2 shows time-dependent resistance data for ROS cells, measured at both 22 and 37°C, when 4 dyn/cm$^2$ of stress was applied and then released. It is apparent that both time-dependent curves demonstrate a viscoelastic-like nature if compared to the theoretical curve in Fig. 1b. For the purpose of fitting the viscoelastic model to the measured

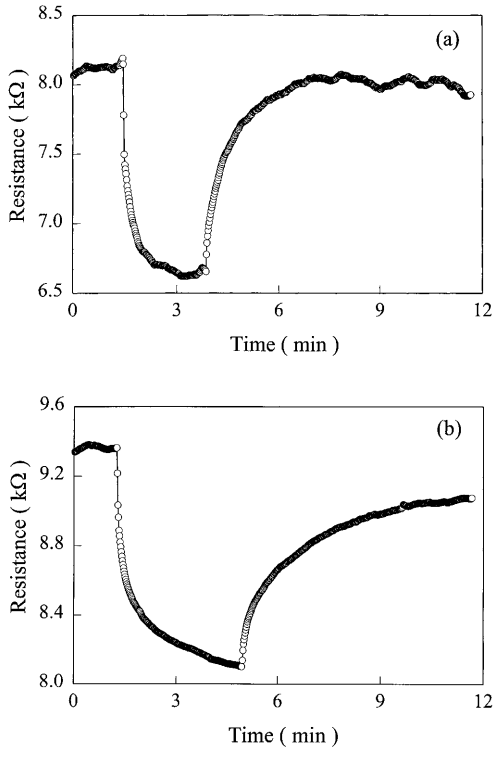


**Fig. 2** Time-dependent resistance measurements on ROS cell layers showing the effect of a step increase in stress (4 dyn/cm$^2$), and then removal of the stress, at **a** 37°C and **b** 22°C. The sampling time between data points is 1 s

time-dependent data, we assume that what happens in 2 s is instantaneous, and obtain the best approximation we can to the longer time constant by assuming there is a single exponential time-dependent process.

To be able to separate fast changes in $R_b$ and $h$ from the slower changes, we carry out an analysis in which measured resistance is plotted versus measured capactive reactance, and then compared to theoretical model calculations made under various assumptions concerning the time-dependence of $R_b$ and $h$. In-phase and out-of-phase voltages are converted to values of resistance ($R$) and capacitive reactance (=$1/2\pi fC$, where $f$ is frequency and $C$ is capacitance), treating the cell-electrode system as a simple series $RC$ circuit. The in-phase and out-of-phase components can then be compared to the in-phase and out-of-phase components from the ECIS model calculations. Physically, $R$ is the sum of the electrode-electrolyte interfacial resistance, the under-the-cells resistance, and the between-the-cells resistance, while $C$ is the capacitance of the electrode-electrolyte interface. Since the junctional resistance between cells ($R_b$) and the average cell-substrate separation ($h$) affect $R$ and $C$ differently (Lo et al. 1995), the time-dependent plot of $R$ versus capacitive reactance (Fig. 3) allows us to say that the quick drop of $R$ in Fig. 2 (particularly the first 2 s after applying force) results from both a decrease of $R_b$ and an increase of $h$, whereas the slow phase of the decrease in $R$ results from a further gradual decrease of $R_b$. This result agrees with the viscoelastic model illus-

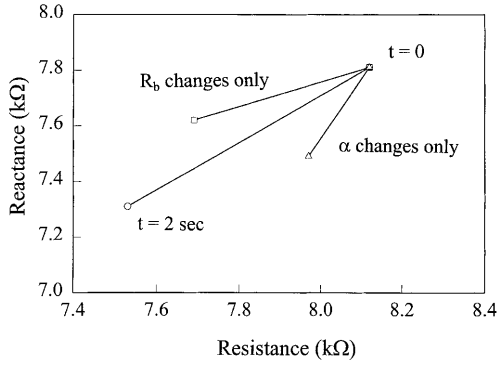


**Fig. 3** A plot of measured capacitive reactance against measured resistance, between $t$=0 (upper right point) and $t$=2 s (lower left point). A theoretical point can be matched to the measured point at $t$=0 by using values for $R_b$ and $\alpha$ that are based on frequency scan data from $t$<0 ($R_b$, $\alpha$=1.5 Ω cm$^2$, 5.8 Ω$^{1/2}$ cm). $R_b$ and $\alpha$ [= $r_c(\rho/h)^{1/2}$] are the key parameters in the ECIS analysis (Lo et al. 1995, 1998). A theoretical estimate for the measured lower left point can be obtained by using an $R_b$ value from frequency scan data at $t \gg \tau$ and the change in measured $R$ from $t$=2 s to $t \gg \tau$, assuming that all of the change in $R$ during this interval is attributable to a change in $R_b$, and also using an α obtained from the frequency scan data at $t \gg \tau$ ($R_b$, $\alpha$=1.2 Ω cm$^2$, 5.5 Ω$^{1/2}$ cm). This point agrees almost exactly with the measured point, demonstrating that virtually all of the change in $R$ following $t$=2 s results from a change in $R_b$. Furthermore, if it is assumed that $\alpha$ does not change during the first 2 s of stress application, the plot shown above the measured one is obtained, while if it is assumed that $R_b$ does not change during these first 2 s, the plot shown below the measured one is obtained. This demonstrates that both $R_b$ and $\alpha$ change during these first 2 s. It should be noted that $h=\rho(r_c/\alpha)^2$, so that a change in α is equivalent to a change in $h$, the cell-substrate separation distance

trated in Fig. 1a. In other words, when constant stress is applied to our adherent cells, in addition to a fast increase of cell-substrate separation, $\Delta h$, there is a fast vertical height increase for the cell body, $\Delta H(0)$, followed by a slower vertical height increase, $\Delta H(t)$. These changes in $H$ produce changes in the distance between the cells, resulting in changes in $R_b$.

Frequency scan measurements were done before stress application and during stress application at $t \gg \tau$, giving $h$ and $R_b$ values for $t$<0 and for $t \gg \tau$. (A detailed example of obtaining $R_b$ and $h$ via a frequency scan measurement is shown in Lo et al. 1998.) Since the slower change in $R$ results from a change in $R_b$, the fast change in $R_b$ can then be obtained from the measured time course for $R$: $R_b(2\text{ s}) = R_b(t \gg \tau) + A[R(2\text{ s}) - R(t \gg \tau)]$.

Table 1 shows the frequency scan results from the same ROS cells used for the time-dependent measurements of $R$ shown in Fig. 2, under two different stress levels, at both 22 °C and 37 °C. The temperature-dependence of $R_b$, measured with or without applied force, almost entirely results from the temperature-dependence of the resistivity of the culture medium ($\rho$=70 and 54 Ω cm at 22 and 37 °C). This indicates that both cell shape and size are similar at the two temperatures (i.e., $l/w$ is similar), although the average cell-substrate separation, $h$, increases as the temperature decreases. However, comparing to our previous $R_b$ and $h$ data for ROS cells without beads (Lo et al. 1998), we see that

**Table 1** Effect of force and temperature on junctional resistance, $R_b$, and cell-substrate separation, $h$, of ROS cells[a]

| | 37°C | | 22° | |
|---|---|---|---|---|
| | $R_b$ (Ω cm$^2$) | $h$ (nm) | $R_b$ (Ω cm$^2$) | $h$ (nm) |
| $\sigma$ = 0 | 1.4 | 41 | 1.7 | 66 |
| $\sigma$ = 4 dyn/cm$^2$ ($t$ = 2 s) | 1.2 | | 1.5 | |
| $\sigma$ = 4 dyn/cm$^2$ ($t \gg \tau$) | 0.7 | 46 | 1.1 | 77 |
| $\sigma$ = 7 dyn/cm$^2$ ($t$ = 2 s) | 1.1 | | 1.4 | |
| $\sigma$ = 7 dyn/cm$^2$ ($t \gg \tau$) | 0.5 | 50 | 0.8 | 87 |

[a] Frequency scan measurements were done before force application ($\sigma$ = 0) and during force application after reaching steady state ($t \gg \tau$), allowing $R_b$ and $h$ to be obtained for both conditions. Since $R_b$ is defined as a specific resistance, it is calculated as the between-the-cells resistance multiplied by electrode area, $A$. We obtain $R_b$ at 2 s as $R_b(t \gg \tau) + A[R(2\text{ s}) - R(t \gg \tau)]$, where $R(t)$ is the measured time-dependent resistance

**Table 2** Elastic modulus of cell-substrate adhesion, $k_0$[a]

| | $\sigma$ (dyn/cm$^2$) | $\Delta h/H$ ($10^{-3}$) | $k_0$ ($10^3$ dyn/cm$^2$) |
|---|---|---|---|
| 37 °C | 4 | 1.25 | 3.20 |
| 37 °C | 7 | 2.25 | 3.11 |
| 22 °C | 4 | 2.75 | 1.45 |
| 22 °C | 7 | 5.25 | 1.33 |

[a] The $\Delta h$ values are from Table 1. Eq. (1a) is used to obtain $k_0$, with $H$ = 4 μm

the cells might lose part of their cell-substrate and cell-cell adhesion during bead binding, since both cell-substrate and cell-cell distances increase after loading collagen-coated magnetic beads.

From the ECIS data of Table 1 and Fig. 2, the viscoelastic parameters, $k_0$, $k_1$, $k_2$, and $\eta$, can be calculated by using Eqs. (1) and (6), and the results are shown in Tables 2 and 3. Table 4 displays the average viscoelastic parameters from five independent measurements, at two temperatures, and at two stress levels. At a given stress, as the temperature decreases our results show a small increase in the elastic moduli of the cell body ($k_1$ and $k_2$), and a larger increase in the viscosity ($\eta$) of the cell body. This is in agreement with the results of Evans and Yeung (1989), who found a two-fold increase in the cell body viscosity of granulocytes as the temperature decreased from 37 °C to 23 °C, using the micropipette aspiration technique (although their viscosity values are much lower than ours). In addition, we see that cell-substrate adhesion strain at a given stress increases as the temperature decreases, giving an elastic modulus of cell-substrate adhesion that is lower at the lower temperature (Table 4), which is as described in our previous study (Lo et al. 1998). Also, at a given temperature, the $k$ values obtained at our two stress levels are fairly

**Table 3** Elastic moduli, $k_1$ and $k_2$, and viscosity, $\eta$, of the cell body[a]

| | $\sigma$ (dyn/cm$^2$) | Time | $\Delta H/H$ ($10^{-3}$) | $k_1$ ($10^3$ dyn/cm$^2$) | $k_2$ ($10^3$ dyn/cm$^2$) | $\tau$ (s) | $\eta$ ($10^5$ $P$) |
|---|---|---|---|---|---|---|---|
| 37 °C | 4 | 2 s | 0.32 | | | | |
| 37 °C | 4 | $t \gg \tau$ | 1.93 | 2.07 | 10.43 | 60 | 1.04 |
| 37 °C | 7 | 2 s | 0.53 | | | | |
| 37 °C | 7 | $t \gg \tau$ | 3.47 | 2.02 | 11.18 | 90 | 1.54 |
| 22 °C | 4 | 2 s | 0.27 | | | | |
| 22 °C | 4 | $t \gg \tau$ | 1.12 | 3.57 | 11.23 | 80 | 2.17 |
| 22 °C | 7 | 2 s | 0.44 | | | | |
| 22 °C | 7 | $t \gg \tau$ | 2.32 | 3.02 | 12.88 | 150 | 3.67 |

[a] The $\Delta H/H$ values are calculated from Eq. 6, using the $R_b$ values from Table 1. We also assume that $H \gg l$, so that $\beta$=1. Our estimates for $H$ and $l$ are 4 and 0.5 μm. Then, $k_1$ and $k_2$ are obtained from Eq. (1b), and $\eta$ is given by $\tau$ and the $k$ values using Eq. (2)

**Table 4** Summary of measured viscoelastic properties of adherent ROS cells[a]

| | $\sigma$ (dyn/cm$^2$) | $k_0$ ($10^3$ dyn/cm$^2$) | $k_1$ ($10^3$ dyn/cm$^2$) | $k_2$ ($10^3$ dyn/cm$^2$) | $\eta$ ($10^5$ $P$) |
|---|---|---|---|---|---|
| 37 °C ($n$ =5) | 4 | 3.2 ± 1.4 | 2.2 ± 1.0 | 10.1 ± 7.3 | 1.0 ± 0.4 |
| 37 °C ($n$ = 5) | 7 | 3.0 ± 0.7 | 2.0 ± 1.1 | 11.0 ± 5.8 | 1.4 ± 0.5 |
| 22 °C ($n$ = 5) | 4 | 1.5 ± 0.4 | 3.6 ± 1.5 | 11.8 ± 6.4 | 2.1 ± 0.7 |
| 22 °C ($n$ = 5) | 7 | 1.3 ± 0.5 | 3.1 ± 1.2 | 13.2 ± 8.5 | 3.7 ± 1.0 |

[a] The values in this table are mean ± standard deviation for five independent measurements at each temperature and stress level

close, but the time constants and viscosity values are noticeably larger at higher stress.

The reason for using the time course of resistance following force application for analysis, rather than the phase following removal of the force, is that our cells show signs of nonlinearity. As indicated above, the stress level affects the measured time constant and viscosity, which is a nonlinear behavior. Furthermore, the time constant of the curve following force removal is dependent on the duration of applied force, which is also indicative of nonlinear viscoelastic behavior (Locket 1972; Haddad 1995). Nonlinear behavior is not surprising for the topologically complex cytoskeleton, in which the spatial relationships of the molecular components (actin filaments, intermediate filaments, and microtubules) will change with changes in strain, and in which breaking and remaking of linking bonds can also occur. Furthermore, there is a biological dimension, in which the cell could be actively reacting to the applied stress, and modifying the various cytoskeletal elements. For example, in fibroblasts, within 30 min under constant stress there is an increase in the number of actin filaments attached to the points of force application, and in the number of cross-links between them (Glogauer et al. 1997, 1998).

The measurement of cellular viscoelastic parameters is no doubt dependent to some extent on the method of stress and strain application. Recent studies on cell body vicoelasticity include that of Thoumine and Ott (1997), in which a fibroblast is seized between two glass microplates, and that of Sato et al. (1996), in which a suspended endothelial cell is partially aspirated into a micropipette. Neither of these studies uses cells that are attached to a substrate via the normal adhesion system as in our method, in which the cells are allowed to attach to the substrate via integrin-fibronectin and integrin-vitronection adhesion bonds over a period of 24 h before measurements are carried out (Lo et al. 1998). The measurements of Thoumine and Ott are carried out between 6–60 min after the cells adhere to the glass microplates, and the measurements of Sato et al. are done on cells in suspension. Furthermore, our method should give a more precise measurement of stress and strain than other methods (Glogauer and Ferrier 1998; Lo et al. 1998).

Nevertheless, the results from these other viscoelastic studies are not completely dissimilar to ours. The results of Sato et al. for the cell body $k$ values and $\eta$ are smaller than ours by about a factor of 10, but their measured retardation time constant is almost the same as ours (their $\tau \approx 125$ s at 22°C). The results of Thoumine and Ott are of the same order of magnitude as ours for both of the cell body $k$ values and for $\eta$, but their $k$ for the element in series with the dashpot is about half the other $k$, the reverse of our result. Also, their time constant is 2–3 times lower than ours, but this is almost exactly as would be expected, since they are measuring a stress relaxation time constant, whereas we (and Sato et al.) are measuring a strain retardation time constant [i.e., $\tau_{\text{retardation}} = \tau_{\text{relaxation}}(k_2+k_1)/k_1$]. The moduli and the viscosity of Sato et al., and the viscosity of Evans and Yeung (1989), may be smaller than ours and those reported by Thoumine and Ott because the micropipette aspiration method involves a larger degree of cellular distortion and possible cytoskeletal disruption. Another possible contributing factor to the lower $k$ values of Sato et al. is that cells in suspension may have a weaker cytoskeleton than cells adhering to a surface.

However, it is not possible at present to predict how much disruption a given measurement technique may produce, or how being in suspension may affect the cytoskel-

eton. The theory of the mechanical properties of the cytoskeleton is poorly understood, with details of the integration of the molecular elements of the cytoskeleton into the submembrane cortex as well as into the whole cell structural system almost completely unknown (Janmey 1991; Glogauer et al. 1997; Lo et al. 1998). Whole cell measurements such as ours can provide estimates of global mechanical parameters for the cell, but cannot address these localized subcellular properties. For example, we do not know what our measured viscosity represents: it may have something to do with unfolding of some cytoskeletal elements, or with the breaking and remaking of cross-links between cytoskeletal elements, or with something else. The spring constants are likely to represent some properties of the actin filaments, but the intermediate filaments and microtubules may also contribute to the global elasticity.

The measured viscoelastic parameters are also dependent on the particular viscoelastic model employed. To explore the degree to which our results are dependent on the viscoelastic model, we applied the simplest model based on a Kelvin-Voigt body, in which the dashpot is in parallel rather than in series with a spring, as in a Maxwell body. The other spring is then in series with the Kelvin-Voigt body, rather than being in parallel with the Maxwell body (Locket 1972; Haddad 1995). The spring in series with the dashpot in our Maxwell model transforms into the spring in series with the Kelvin-Voigt body; using our measured parameters at 37 °C and 4 dyn/cm$^2$, its spring constant increases by 22% [the conversion factor is $\gamma=(k_1+k_2)/k_2=1.22$]. The other spring constant also increases by 22% (the same conversion factor), while the viscosity increases by 49% (the conversion factor is $\gamma^2$). This shows that the measured parameters are sensitive to the particular model used, but that the order of magnitude is the same with either viscoelastic model.

In summary, we are able to estimate viscoelastic parameters for the cell body by measuring changes in cellular strain in response to applied stress, by using ECIS. Time-dependent and frequency-dependent impedance measurements allow us to estimate the time course of strain in the cell body, as well as strain in the cell-substrate adhesion system. By comparing the time dependence of strain estimated by these impedance measurements to a viscoelastic model, the elastic and viscous parameters of the model can be obtained. It is not yet clear how the various cytoskeletal elements produce the various aspects of the viscoelastic properties exhibited by the cell body in measurements such as reported here. Clearly, to further explain the mechanical properties of the cell body, even more complex (nonlinear) viscoelastic models must be used, combined with further measurements and analysis under a range of stress levels and durations, and under various conditions of cytoskeletal disruption.

## References


Chen CS, Mrksich M, Huang S, Whitesides GM, Ingber DE (1997) Geometric control of cell life and death. Science 276:1425–1428

Elson EL (1988) Cellular mechanics as an indicator of cytoskeletal structure and function. Annu Rev Biophys Chem 17:397–430

Evans E, Yeung A (1989) Apparent viscosity and cortical tension of blood granulocytes determined by micropipet aspiration. Biophys J 56:151–160

Ferrier J, Ward-Kesthely A, Homble F, Ross S (1987) Further analysis of spontaneous membrane potential activity and the hyperpolarizing response to parathyroid hormone in osteoblastlike cells. J Cell Physiol 130:344–351

Giaever I, Keese CR (1991) Micromotion of mammalian cells measured electrically. Proc Natl Acad Sci USA 88:7896–7900

Glogauer M, Ferrier J (1998) A new method for application of force to cells via ferric oxide beads. Pflügers Arch 435:320–327

Glogauer M, Arora P, Yao G, Sokholov I, Ferrier J, McCulloch CAG (1997) Calcium ions and tyrosine phosphorylation interact coordinately with actin to regulate cytoprotective responses to stretching. J Cell Sci 110:11–21

Glogauer M, Arora P, Chou D, Janmey PA, Downey GP, McCulloch CAG (1998) The role of actin-binding protein 280 in integrin-dependent mechanoprotection. J Biol Chem 273:1689–1698

Haddad YM (1995) Visoelasticity of engineering materials. Chapman and Hall, New York, pp 33–69, 142–166

Ingber DE, Dike L, Hansen L, Karp S, Liley H, Maniotis A, McNamee H, Mooney D, Plopper G, Sims J (1994) Cellular tensegrity: exploring how mechanical changes in the cytoskeleton regulate cell growth, migration, and tissue pattern during morphogenesis. Int Rev Cytol 150:173–224

Janmey PA (1991) Mechanical properties of cytoskeletal polymers. Curr Opin Cell Biol 2:4–11

Korn GA, Korn TM (1967) Manual of mathematics. McGraw-Hill, New York, p 245

Lo C-M, Ferrier J (1998) Impedance analysis of fibroblastic cell layers measured by electric cell-substrate impedance sensing. Phys Rev E 57:6982–6987

Lo C-M, Keese CR, Giaever I (1994) pH changes in pulsed $CO_2$ incubator cause periodic changes in cell morphology. Exp Cell Res 213:391–397

Lo C-M, Keese CR, Giaever I (1995) Impedance analysis of MDCK cells measured by electric cell-substrate impedance sensing. Biophys J 69:2800–2807

Lo C-M, Glogauer M, Rossi M, Ferrier J (1998) Cell-substrate separation: effect of applied force and temperature. Eur Biophys J 27:9–17

Locket FJ (1972) Nonlinear viscoelastic solids. Academic Press, New York, pp 59–73

Lotz MM, Burdsal CA, Erickson HP, McClay DR (1989) Cell adhesion to fibronectin and tenascin: quantitative measurements of initial binding and subsequent strengthening response. J Cell Biol 109:1795–1805

Majeska RJ, Rodan GA (1982) The effect of $1,25(OH)_2D_3$ on alkaline phosphatase in osteoblastic osteosarcoma cells. J Biol Chem 257:3362–3365

Sato M, Ohshima N, Nerem RM (1996) Viscoelastic properties of cultured porcine aortic endothelial cells exposed to shear stress. J Biomech 29:461–467

Schmid-Schönbein GW, Sung KLP, Tözeren H, Skalak R, Chien S (1981) Passive mechanical properties of human leukocytes. Biophys J 36:243–256

Thoumine O, Ott A (1997) Time scale dependent viscoelastic and contractile regimes in fibroblasts probed by microplate manipulation. J Cell Sci 110:2109–2116